Behavior of CIII to CVI emissions during recombining phase of LHD plasmas

Malay Bikas Chowdhuri, Shigeru Morita[a] and Motoshi Goto[a]

Department of Fusion Science, Graduate University for Advanced Studies,

Toki 509-5292, Gifu, Japan

[a] *National Institute for Fusion Science, Toki 509-5292, Gifu, Japan*

(Received 15 October 2007 / Accepted 15 October 2007)

Carbon emissions of CIII-CVI during recombining phase of the Large Helical Device (LHD) plasma are studied to understand their behaviors. For the purpose four resonance transitions of CIII (977Å: $2s^2\ ^1S$-$2s2p\ ^1P$), CIV (1550Å: $2s\ ^2S$-$2p\ ^2P$), CV (40.27Å: $1s^2\ ^1S$-$1s2p\ ^1P$) and CVI (33.73Å: $1s\ ^2S$-$2p\ ^2P$) are observed using absolutely calibrated VUV monochromators and EUV spectrometers. One dimensional impurity transport code has been used to calculate the spectral emissivity under the consideration of measured n_e and T_e profiles. The temporal evolution of line emissions have been calculated and compared with the measured data. The comparison shows that the carbon density is 3% to n_e. However, the discrepancy between the calculated and measured values has been noticed in CIII and CIV. It has been argued that three dimensional structures of CIII and CIV emissions are likely to be the reason for this difference, which is based on the presence of relatively high-density and high-temperature plasmas in edge ergodic layer in LHD. It is also found that the CVI emission during recombining phase increases with n_e whereas it is nearly constant during steady state phase suggesting the disappearance of the edge particle screening effect.

Keywords: impurity, carbon, intensity computation, recombining phase.

1. Introduction

For the study of the impurity behavior in high temperature plasmas impurity densities in each charge state are usually analyzed using spectral absolute intensities measured from spectroscopic diagnostics in combination with a one-dimensional impurity transport code [1]. It evaluates radial profiles of charge state and emissivity based on measured electron density and temperature profiles. In general the impurity transport studies have been done during the steady-state phase of discharges using either of intrinsic or extrinsic impurity particles [2-5]. When the impurity time behavior is analyzed at the transient phase, especially the plasma termination phase, the time duration is very short in the case of tokamaks because of the abrupt disruption after the current termination. Even if the toroidal current is controlled for the smooth termination of the plasma, the magnetic field topology and resultant magnetic surface structure change so much as a function of time. In stellarator cases, on the other hand, the magnetic field for the confinement is externally supplied and maintains steadily even during the transient phase of the discharges. The temporal evolution of impurity emissions from such plasmas can be easily computed under the presence of steady magnetic surface.

In the Large Helical Device (LHD) the helical magnetic field for the plasma confinement produced by superconducting magnetic coils makes possible the steady state operation. The analysis is of course possible on the transient period at initial and final phases of the discharges. In such period the temporal variation of electron and ion densities is mainly governed by atomic ionization and recombination processes instead of the particle transport [6]. Therefore, the absolute intensities of edge spectral lines emitted from fueling gas and impurities can be basically converted to respective ion densities even if the edge temperature and density profiles are not measured in detailed. In this paper temporal behavior of edge carbon emissions is studied during the recombining phase of LHD discharges and the carbon density measurement is attempted with analysis of the carbon emissions as a function of n_e.

2. Experimental Setup

The experiment has been conducted with inwardly shifted configuration of R_{ax}=3.6m and B_t= 2.75T. A discharge is initiated by electron cyclotron heating (ECH)

author's e-mail: chowdhuri.malayl@nifs.ac.jp

and the plasma is sustained by three negative-ion-based neutral bean injection (NBI) devices. Several spectroscopic diagnostics covering visible to X-ray wavelength ranges have been installed to monitor and study the impurity behaviour of LHD discharges. In the present study emissions from different ionization stages of carbon have been measured using two extreme ultra violet (EUV) spectrometers [7, 8] and two vacuum ultra violet (VUV) monochromators [9]. Two absolutely calibrated EUV spectrometers cover 10–130Å (EUV_Short) and 50–500Å (EUV_Long) wavelength range, respectively. Back-illuminated VUV sensitive charge couple device (CCD) detectors are mounted with two EUV spectrometers and operated in full binning mode. Data from the CCD have been acquired in every 5 ms. Four resonance transitions of CIII (977Å, $2s^2\ ^1S$-$2s2p\ ^1P$), CIV (1548Å, $2s\ ^2S$-$2p\ ^2P$), CV (40.27Å, $1s^2\ ^1S$-$1s2p\ ^1P$) and CVI (33.73Å, $1s\ ^2S$-$2p\ ^2P$) are mainly monitored for this study. The CV and CVI emissions are measured using the EUV_Short spectrometer with a spectral resolution of ~0.10Å at 40Å. The resonance transitions from Li- and Be-like carbon ions are observed using two 20cm normal incidence VUV monochromators equipped with an electron multiplier tube detector. The signal is acquired with time interval of 100μs. The two VUV monochromators were absolutely calibrated using the carbon emissions by comparing the raw signals with the absolutely calibrated EUV_Long spectrometer for 50–500Å. Two experimental intensity ratios of $2s^2$-2s3p (386.4Å) to $2s^2$-2s2p (977Å) transitions from CIII and of 2s-3p (312.4Å) to 2s-2p (1550Å) transitions from CIV were adopted for the calibration. Electron temperature and density profiles measured with Thomson diagnostics and line-integrated electron density measured with FIR diagnostics are used for the present analysis.

3. Description of Calculation

Analysis on temporal behaviors of carbon emissions in different ionization stages are based on the calculation of the line-integrated emissivity using one-dimensional impurity transport code [1]. The time behavior of the impurity density profile is calculated by the following equation with the ionization balance of an impurity ion;

$$\frac{\partial n_q}{\partial t} = -\frac{1}{r}\frac{\partial}{\partial r}\left(r\Gamma_q\right) + \alpha_{q-1} n_{q-1} n_e + \beta_{q+1} n_{q+1} n_e - \left(\alpha_q + \beta_q\right) n_q n_e \qquad (1)$$

where n_q and Γ_q are the ion density and particle flux of qth charge state, respectively. The parameters of α and β represent the ionization and recombination rate coefficients, respectively. The empirical transport model [10], of which the validity was confirmed in LHD, using the diffusion coefficient D and convective velocity V is given by;

$$\Gamma_q = -D_q(r)\frac{\partial n_q}{\partial r} + V_q(r) n_q \qquad (2)$$

$$\text{and} \quad V_q(r) = -V(a)\frac{r}{a}. \qquad (3)$$

Here, a, D_q and V_q are the plasma radius, diffusion coefficient and convective velocity, respectively.

After the charge state calculation the emissivity and brightness profiles of emission line was evaluated. The emissivity of transition from level j to i, $\varepsilon(i,j)$, is expressed by the relation of $\varepsilon(i, j) = N_q(j)A(i, j)$, where A(i, j) is the transition probability and $N_q(j)$ is the density of the level j in charge state q. The emissivity is calculated from the level-population in the upper level. The level-population is generally determined by the collisional and radiative processes among several quantum levels [11]. However, the coronal model is assumed in the present case for the simplicity. This assumption really gives a good agreement with the C-R model calculation, at least, for the H- and He-like systems. Therefore, the relation can be written as $E(i,j) = N_q(j)A(i, j) = n_q n_e Q(i, j)$, where Q(i, j) is the excitation rate coefficient for the transition of i to j. The excitation rate coefficient for individual line has been taken from calculated results by Itikawa et al. [12].

4. Results and Discussions

A typical waveform of NBI discharge used in the present impurity study is shown in Fig.1. The time evolution of carbon emissions has been analyzed at the recombining phase from 2.45s to the end of the plasma termination, where the T_e quickly decreases due to the absence of the heating source while the n_e stays constant. The central electron temperature $T_e(0)$ measured by Thomson scattering diagnostic was available until t=2.620s. The CV and CVI emissions, on the other hand, dropped to zero at 2.628s, and the CIII and CIV emissions disappeared 15ms later because of their low ionization energies (I.E.) (CIII: 50eV, CIV: 68eV, CV: 367eV and CVI: 475eV). Extrapolation of the measured T_e was therefore necessary to calculate the emissivity of the carbon emissions in different ionization stages. The T_e was calculated from magnetic energy and line-integrated electron density $\langle n_e \rangle$. The measured and extrapolated $T_e(0)$ and plasma radius r_b at horizontally elongated plasma cross section are plotted in Fig.2. The $T_e(0)$ and the plasma radius gradually decrease, and after t=2.550s the $T_e(0)$ begins to drop quickly. The CIII and CIV emissions also start to increase rapidly at t=2.550s.

Temporal evolution of carbon emissions during the recombining phase has been calculated using one-dimensional impurity transport code. The calculation has been done on the averaged magnetic surface by

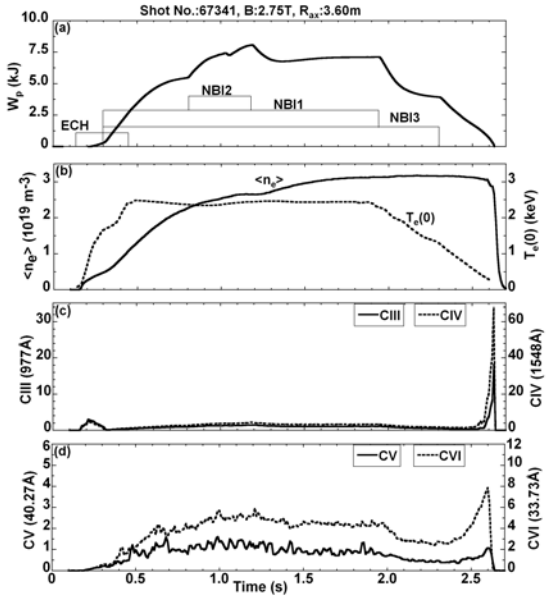

Fig.1 Typical discharge for the present analysis; (a) plasma stored energy and heating pulses, (b) line-averaged electron density (solid line) and central electron temperature (dashed line), (c) CIII (solid line) and CIV (dashed line) emissions and (d) CV (solid line) and CVI (dashed line) emissions. All carbon emissions have unit of 10^{14} photons.cm^{-2}.sr^{-1}.s^{-1}. Data between t=2.45s to 2.65s are used for analysis.

replacing the elliptical shape of LHD plasmas with the circular shape. In this study the diffusion coefficient D_q is considered as an independent of q and r, and the inward convection velocity V_q is as a function of r. Here, the maximum value of V_q is given as V(a) at average plasma radius a (see Eq.3). The values of D_q and V(a) are taken to be $0.2m^2s^{-1}$ and $1.0ms^{-1}$ for the diffusion coefficient and inward convective velocity, respectively.

Figure 3 illustrates the total radiation power emitted from Be-like CIII to H-like CVI, which are obtained by integrating the whole plasma surface of LHD. The experimental and calculated results are indicated with solid and dashed lines, respectively. In the calculation 3% carbon density is assumed to the electron density. All the carbon radiations gradually increase after turning off the heating power as the T_e decreases. At first the CVI emissions reach the peak value at 2.60s where the $T_e(0)$ is 280eV. This is in good agreement with the calculation. Then, the CV and CVI radiations quickly decrease and become zero immediately at 2.625s. At this moment the $T_e(0)$ drops less than 150eV. The calculation of CV and CVI radiations also drop at 2.630s. Since the exposure time of CCD detector is 5ms in the present experiment, the difference between the measurement and calculation may originate in the uncertainty of the time window.

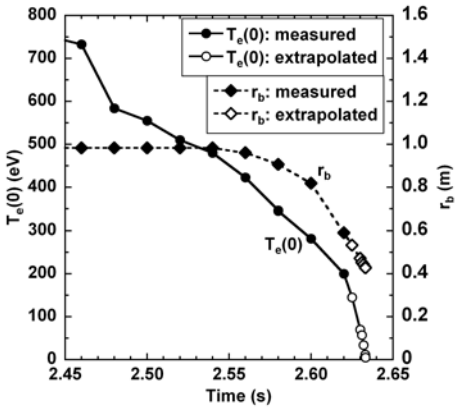

Fig.2 Time behaviors of central electron temperature ($T_e(0)$: circles) and horizontal plasma radius (rb: diamonds) at horizontally elongated plasma cross section during recombining phase. Closed circles and diamonds means measured values, and open circles and diamonds mean extrapolated values.

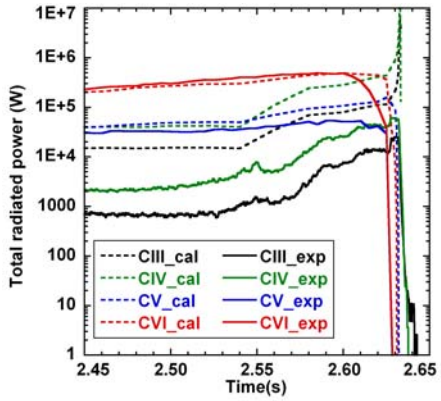

Fig.3 Calculated and experimental total radiation power of CIII to CVI. Dash and solid lines indicate calculated and experimental data.

On the other hand, dynamic range of the CIII and CIV emissions is really large compared to the CV and CVI cases. The voltage applied to the SEM is always adjusted to monitor the main discharges, not the plasma termination phase. Then, the signals of CIII and CIV are always saturated at the plasma termination phase as seen during t=2.628-2.632s in the figure. The calculation of CIII and CV radiations reach the peak value at 2.632s when the $T_e(0)$ becomes 12eV. The calculation after 2.633s is, however, impossible in practice, because of the extremely low electron temperature. In the discharge very low temperature plasma is maintained until t=2.645s as apparently seen in the CIII temporal behavior.

During steady-state phase of discharges the carbon emissions are basically located inside the narrow shell at plasma edge. In LHD the CIII and CIV generally exist in

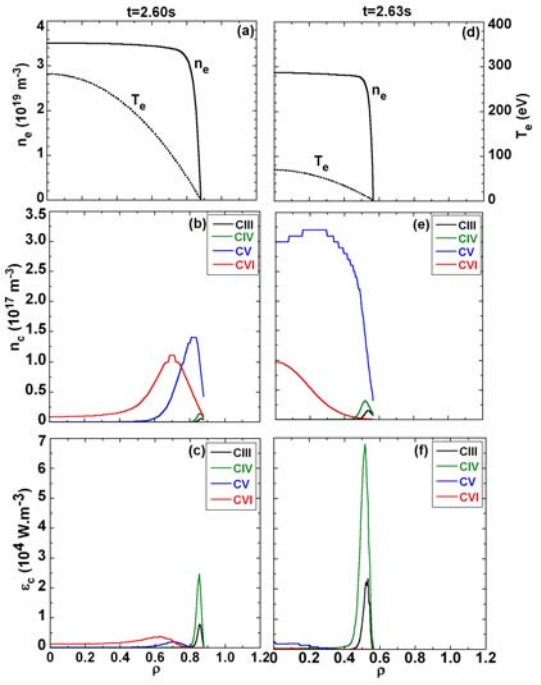

Fig.4 Radial profiles of n_e and T_e ((a) and ((d)), densities ((b) and (e)) and emissivities ((c) and (f)) of CIII to CVI taken at two different time frames of 2.60s (a, b and c) and 2.63s (d, e and f). Abscissa means normalized radius, ρ.

the ergodic layer [13] surrounding the main plasma and the CV and CVI exist near the last closed flux surface (LCFS). During recombining phase the width of the emission shells is broaden as the T_e decreases, and moves inside because of the reducing plasma size, as shown in Fig.2. Calculated results on the radial profiles of carbon densities and emissivities are shown in Fig.4. Figure 4 (a)-(c) and (d)-(f) are the radial profiles at t=2.60s and 2.63s in Fig.3, respectively. The CVI emission takes the maximum value at 2.60s and the CV and CVI entirely disappear at 2.63s. Fig. 4(a) and (c) are the measured n_e and T_e profiles used in the calculation. The CIII and CIV are always located at the plasma edge in these time frames with sharp peaks.

On the other hand, the CV and CVI emission profiles are quite different. At t=2.60s the shell widths of the CV and CVI densities become wider (see Fig.4 (b)), and resultant emission profiles also become much wider (see Fig.4 (c)). Especially the tendency is remarkable to the CVI emission profile, because the excitation coefficient of CVI quickly drops at T_e<200eV. This effect can be seen in the difference at the peak positions of CVI density and emissivity profiles (ρ=0.67 and 0.63). At t=2.63s the CV and CVI emissions entirely disappear as seen in Fig.4(f), whereas the CV and CVI densities increase at the plasma center (see Fig.4(e)). The excitation rate coefficient of

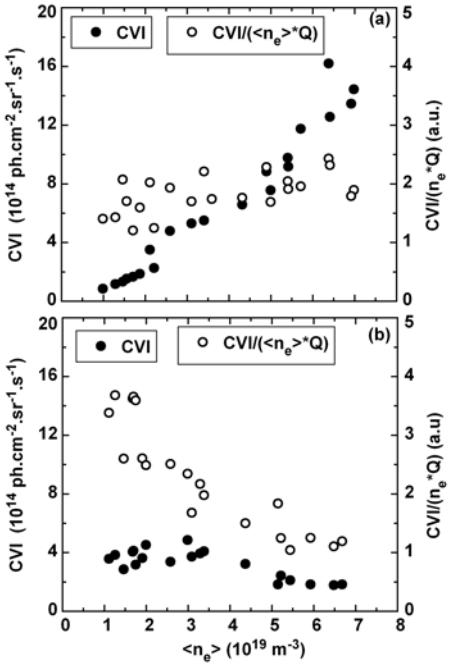

Fig.5 CVI intensity (closed circles) and CVI/(n_e*Q) (open circles) plotted against line-averaged electron density <n_e> for (a) recombining and (b) steady state phases. Value of Q means excitation rate coefficient of CVI.

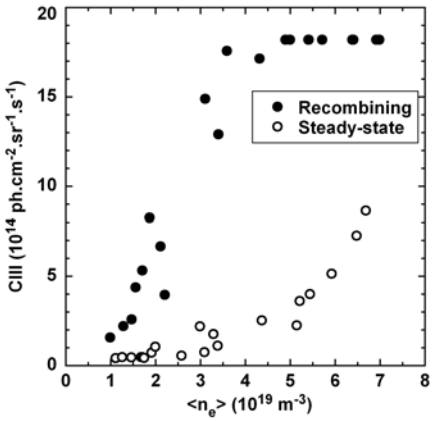

Fig.6 CIII intensity against line-averaged electron density <n_e> for recombining (closed circles) and steady state phases (open circles).

CVI at Fig.4(f) (T_e(0)=70eV) decreases 30 times compared to Fig.4(c) case (6×10^{-17}m^3.s^{-1} at T_e(0)=280eV).

Calculation of the total radiation power from the CV and CVI shows the good agreement with the experiment under assumption of 3% carbon density. However, the CIII and CIV results are ten times larger than the experimental values. The reason is not fully clear at present. At least it is known that the emission distribution from low ionized ions and neutral atoms is toroidally and poloidally inhomogeneous because of the presence of the

ergodic layer. Indeed, recent studies indicate that the emissions from CIII and CIV have the asymmetric features reflecting the field line structure of the ergodic layer [14]. Especially, the vertical profile of CIV exhibits four peaks. The four peaks are formed at the inboard side near the X-point in addition to the top and bottom edge peaks at the horizontally elongated plasma cross section. It is reported that the particle recycling is enhanced at the inboard side [15]. It is also observed that the inhomogeneous poloidal distribution of neutral emissions arises mainly from inhomogeneity in the neutral particle density, not from the nonuniformity of the electron temperature and density [16]. This is likely to be one of the reasons for the difference.

Finally the CVI emission is examined for several discharges at the peak value during the recombining phase, where the plasma begins to shrink and the size becomes a little smaller than the LCFS. The CVI emission during steady-state phase is also studied for the comparison. Intensities of CVI are plotted against $<n_e>$, as shown in Fig. 5(a) and Fig. 5(b) for the recombining and steady state phases, respectively. CVI intensities normalized to the electron density $<n_e>$ and excitation rate coefficient, Q, ($CVI/(n_e*Q)$, which means the carbon density of CVI), are also plotted in the figures. The excitation rate coefficient is calculated against the electron temperature at the LCFS for steady state phase and at the central electron temperature for recombining phase. This choice is reasonably correct since the CVI emission location is estimated from the CV radial profile. The difference between two phases is very clear. The CVI intensities from recombining phase increase with $<n_e>$ but those from steady-state phase decrease with $<n_e>$. Thus, we find a clear difference in the carbon density behavior with $<n_e>$. That is to say, the CVI density is nearly constant with $<n_e>$ for recombining phase, but it definitely decreases with $<n_e>$ for steady state phase. On the other hand, the CIII intensities, which suggest the carbon influx for the ionizing plasma like during steady state phase, increase with $<n_e>$ for both phases, as shown in Fig.6. The CIII intensities for recombining phase are saturated at densities greater than 5×10^{19} m^{-3}. The reduction of the CVI density for steady state phase may suggest the impurity screening effect. Increasing the density in the ergodic layer, the friction force becomes large, which leads to the impurity screening. In case of the recombining phase the understanding of carbon emissions is not really simple, because the CIII emissions do not indicate simply the influx. In addition, the origin of the carbon source is very unclear since the plasma shrinks and is completely detached from the divertor plates and vacuum wall. We need further investigation on the study of carbon behavior during the recombining phase.

4. Summary

Temporal evolution of carbon emission during the recombining phase of the discharges has been studied through the calculation of spectral emissitvity using 1-d transport code. From the calculation of CV and CVI radiation it indicates that carbon density is 3% of electron density, n_e. The discrepancy between computed and experimental CIII and CIV radiation has been found. Although the reason behind this is not fully clear it is argued that the three dimensional structure of CIII and CIV emissions might be responsible for the differences along with localized sources of carbon. Comparison of CVI emissions during steady state and recombining phase reveal its different dependence with n_e. From this observation it is also suggested that impurity screening effect increases with n_e during the steady state phase and it disappears during the recombining phase of the discharges.

Acknowledgements

The authors would like to thank the members of LHD experimental group for their technical support. This work was carried out partly under the LHD project financial support (NIFS06ULPP527).

[1] T. Amano, J. Mizuno and T. kako, Int. Rep. IIPJ-616, Institute for Plasma Physics, Nagoya University (1982).
[2] J. C. Moreno and E. S. Marmar Phys. Rev. E **31**, 3291 (1985).
[3] H. Chen et al., Plasma Phys. Control. Fusion **43**, 1 (2001).
[4] H. Nozato, S. Morita, M. Goto et al., Phys. Plasmas **11**, 1920 (2004).
[5] R. Burhenn et al., Fusion Sci. Tech. **46**, 115 (2004).
[6] M. Goto, S. Morita et al., Phys. Plasmas **10**, 1402 (2003).
[7] M. B. Chowdhuri, S. Morita, M. Goto et al., submitted to Applied Optics.
[8] M. B. Chowdhuri, S. Morita, M. Goto et al., Rev. Sci. Instrum. **78**, 023501(2007).
[9] S. Morita, M. Goto et al., Physica Script **T91**, 48 (2001).
[10] S. Morita, M. Goto et al., Plasma Sci. Tech. **8**, 55 (2006).
[11] M. Goto, J. Quant. Spect. Rad. Trans. **76**, 331 (2003).
[12] Y. Itikawa et al., Atomic Data and Nuclear Data Tables, **33**, 149 (1985).
[13] S. Morita, T. Morosaki, M. Goto et al., Nucl. Fusion **47**, 1033 (2007).
[14] R. Katai, S. Morita, M. Goto et al., Rev. Sci. Instrum. **77**, 10F307 (2006).
[15] M. Goto and S. Morita. Phys. Rev. E **65**, 026401 (2002).
[16] H. Yamazaki, M. Goto, S. Morita et al., submitted to PFR.